Supporting Information to

Temperature dependence of structure and ionic conductivity of $LiTa_2PO_8$ ceramics

*Ruoyu Dai[a], Maxim Avdeev[b,c], Seung-Joo Kim[d], Rayavarapu Prasada Rao[e], Stefan Adams[a]**

[a] Department of Materials Science and Engineering, National University of Singapore, Singapore 117575, Singapore.

[b] Australian Centre for Neutron Scattering, Australian Nuclear Science and Technology Organisation, New Illawarra Rd, Lucas Heights, NSW 2234, Australia

[c] School of Chemistry, The University of Sydney, Sydney, 2006, Australia

[d] Department of Chemistry, Department of Energy Systems Research, Ajou University, Yeongtong-gu, Suwon 443-749, Korea

[e] Department of Mechanical Engineering, National University of Singapore, Singapore 117575, Singapore.

[*] Email: mseasn@nus.edu.sg

1. **Glass-forming ability of ion conducting oxides**

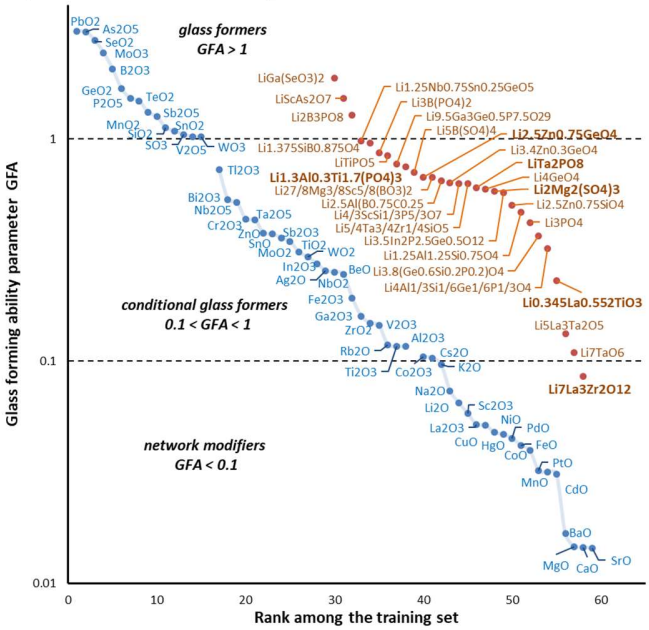

Figure S1. Comparison of Glass forming ability (GFA) of binary oxides (blue symbols) and of a series of known or predicted Lithium-ion conductors. The numeric values of the machine-learned GFA scale is chosen so that oxides with GFA > 1 are glass-formers, oxides with 0.1< GFA < 1 can be classified as conditional glass formers and oxides with GFA < 0.1 act as network modifiers. When applying the same scale to known and literature-predicted Li-ion conducting oxides (brown symbols) an accumulation of ionic conductors is observable near the boundary line between glass formers and conditional glass formers. This includes a variety of LiSICON, NaSICON type ionic conductors, but also sulfates, selenates, arsenates, $LiTa_2PO_8$ etc. Relatively few such as the perovskites and particularly garnets would be classified in the lower half of the "conditional glass former" domain.

2. Crystal structure data from neutron powder diffraction

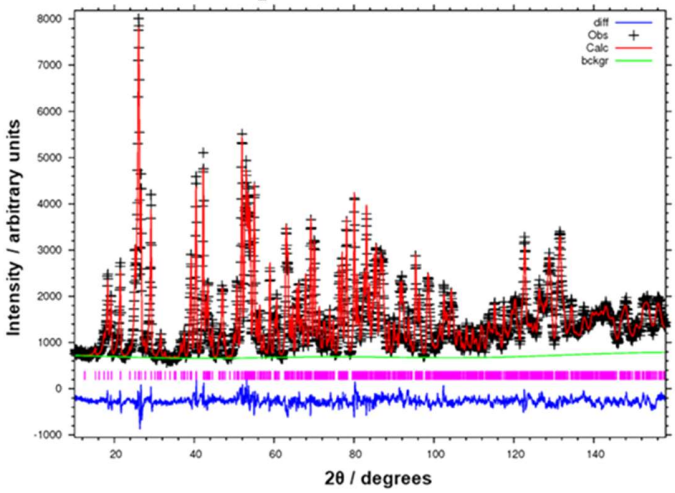

Figure S2. Rietveld refinement of Neutron powder diffraction data of $LiTa_2PO_8$ at T = 3 K. For refinement results see Table S.1 on the following page.

Table S1. Summary of structural information of $LiTa_2PO_8$ determined by neutron powder diffraction (NPD) at T = 3 K.

Empirical formula:	$LiTa_2PO_8$
Formula weight (M_r):	527.81
Space group:	*C*2/*c*
Number of formula units Z	8
Density (g/cm^3)	5.866
Temperature (K)	3
Wavelength (Å)	1.6220
2θ range (°)	10 – 158
2θ step (°)	0.05
No. of refined parameters	60
a (Å)	9.7070(2)
b (Å)	11.5179(2)
c (Å)	10.6909(2)
β (°)	90.216(2)
Volume (Å^3)	1195.28(4)
R_p (%)	4.35
R_{wp} (%)	5.44
$R(F^2)$ (%)	4.10
χ^2	4.55

Atom	**Wyckoff site**	**s.o.f.**	**X**	**Y**	**Z**	**U_i×100 (Å^2)**
Ta1	8*f*	1	0.2470(4)	0.0949(3)	0.2580(4)	-0.19(5)[a)]
Ta2	4*e*	1	0	0.3399(5)	¼	-0.19(5)[a)]
Ta3	4*a*	1	0	0	0	-0.19(5)[a)]
P	8*f*	1	0.4996(6)	0.2101(4)	0.0594(4)	0.19(9) [a)]
O1	8*f*	1	0.0587(5)	0.3325(5)	0.0681(4)	0.66(3) [a)]
O2	8*f*	1	0.3797(5)	0.1345(4)	0.4057(4)	0.66(3) [a)]
O3	8*f*	1	0.3574(5)	0.5055(4)	0.1299(4)	0.66(3) [a)]
O4	8*f*	1	0.0464(5)	0.1641(4)	0.5519(4)	0.66(3) [a)]
O5	8*f*	1	0.1447(5)	0.2374(4)	0.2897(4)	0.66(3) [a)]
O6	8*f*	1	0.1387(5)	0.0580(4)	0.1135(4)	0.66(3) [a)]
O7	8*f*	1	0.3785(5)	0.2009(4)	0.1538(4)	0.66(3) [a)]
O8	8*f*	1	0.1346(5)	0.4655(4)	0.2836(4)	0.66(3) [a)]
Li1	8*f*	0.41(2)[b)]	0.759(3)	0.154(2)	0.653(3)	0.66(3) [a)]
Li2	8*f*	0.31(3)[b)]	0.236(3)	0.359(4)	0.418(4)	-1.5(3) [a)]
Li3	8*f*	0.23(3)[b)]	0.166(7)	0.525(5)	0.498(6)	-1.5(3) [a)]
Li4	8*f*	0.05(3)[b)]	0.347(13)	0.351(14)	0.257(14)	-1.5(3) [a)]

[a)] U_{iso} values for each element were constrained to a single value

[b)] Sum of lithium site occupancy factors (s.o.f.) restrained to 1.

3. XRD patterns of LTPO samples after spark plasma sintering

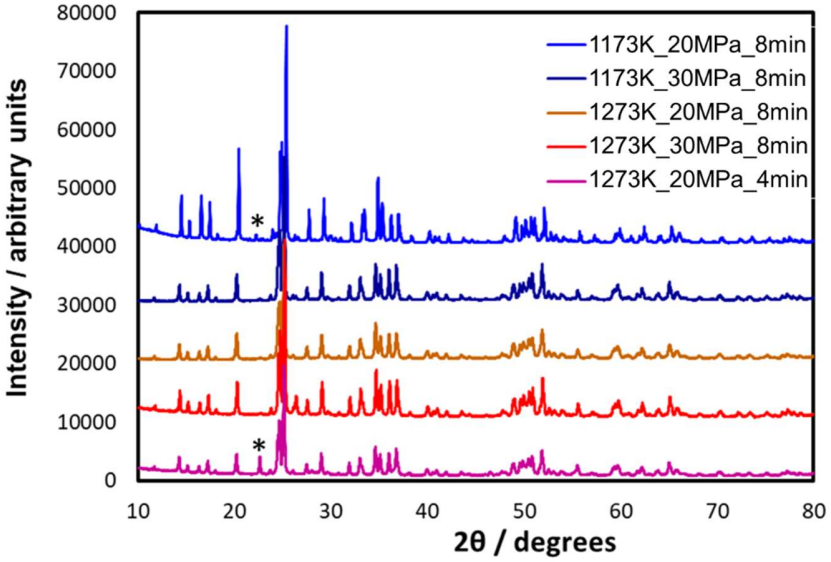

Figure S3. Overview of X-ray powder diffraction data of $LiTa_2PO_8$ samples prepared by ball milling after various sintering conditions. The asterisk refers to impurity peaks of re-formed Li_2CO_3.

4. XRD patterns of LTPO samples produced by rapid grinding technique

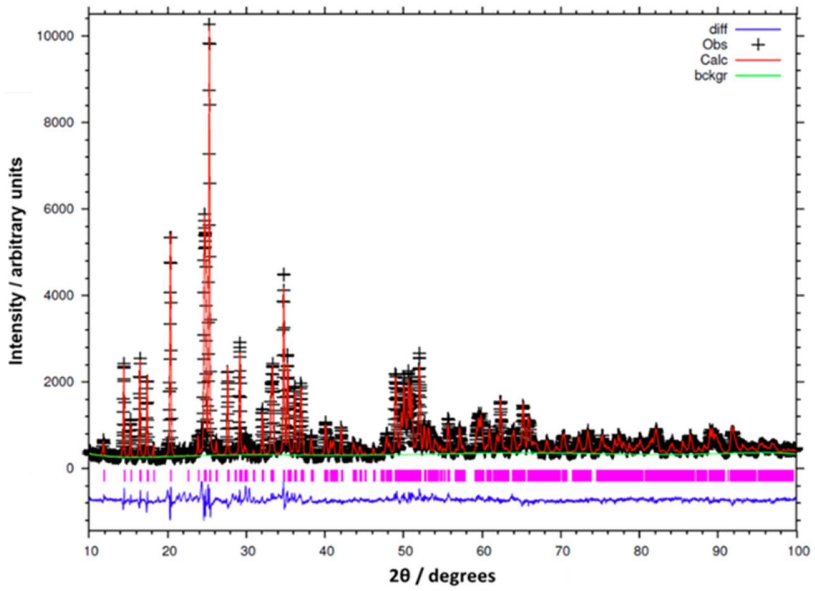

Figure S4. Rietveld refinement of room temperature X-ray powder diffraction data of $LiTa_2PO_8$ prepared by the accelerated grinding approach.

5. Neutron diffraction results on temperature dependence of crystal structure

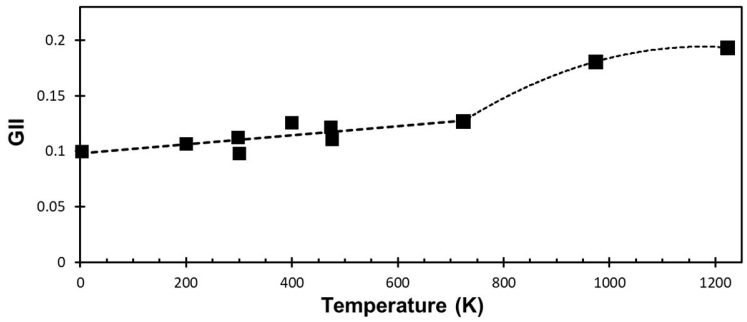

Figure S5. Global instability index (GII) as a measure of the plausibility of the crystal structure models refined from the neutron diffraction data over the temperature range 3 K < T < 1223 K. The global instability index, i.e. the mean squared mismatch of the bond valence sums averaged over all atoms in the crystal structure is nearly stable up to 723 K, while the precision of the (especially Li) atom positions is somewhat lower for the two highest temperatures 973 and 1223 K. For a plausible crystal structure model at room temperature, a value of GII < 0.2 is commonly expected.

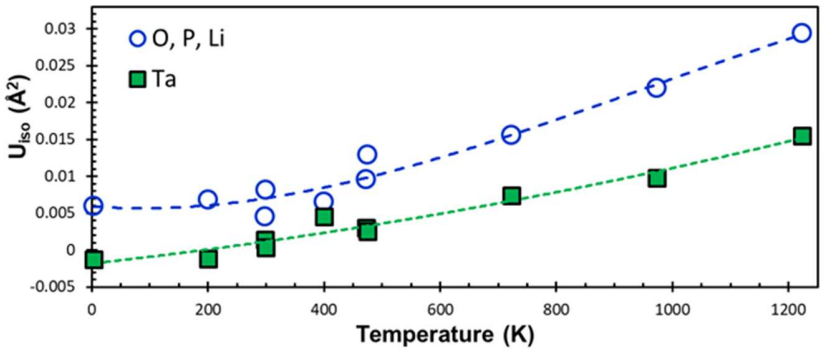

Figure S6. Variation of the atomic displacement parameters U_{iso} of the Ta toms (green squares) and of the lighter atoms O, P or Li (open blue circles) with temperature. To limit the number of refined parameters a common U_{iso} for all Ta atoms as well as a distinct common value for all lighter atoms have been assumed in the Rietveld refinements of neutron powder diffraction data. (Note that this is different from the refinement shown in in Fig. S1 and Table S1, where distinct U_{iso} values were refined for each element). Broken lines refer to 3rd order polynomial fits to the displayed data. While the U_{iso} for Ta within experimental error converge to zero, suggesting that the U_{iso}(Ta) correspond to the Ta atom vibrations, the values for the lighter atoms are practically constant up to 400 K, suggesting a significant contribution of static disorder to U_{iso} for the light atoms.

6. Impedance spectra of LTPO

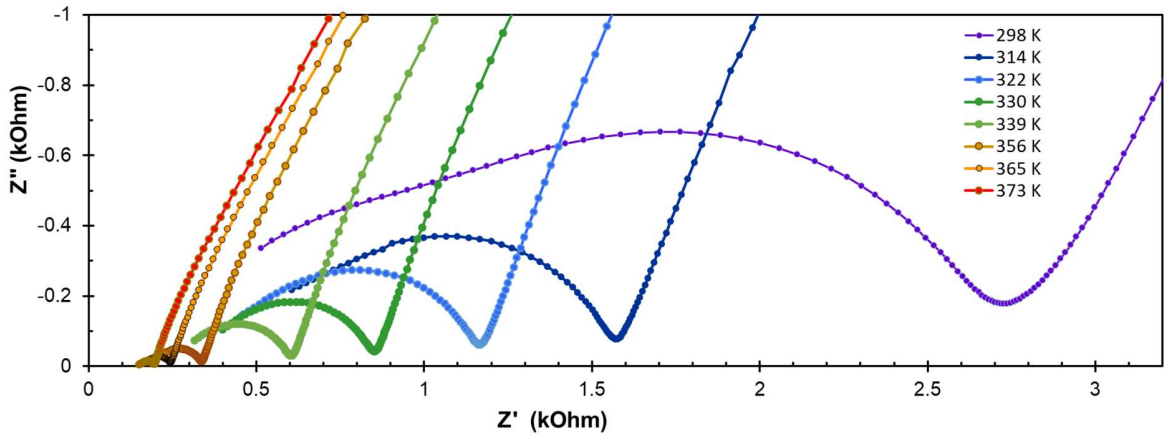

Figure S7. Selected Nyquist plots of electrochemical impedance spectra for $LiTa_2PO_8$ over the temperature range 298 – 373 K. Data analysis assumed an equivalent circuit of $(R_{bulk}Q_{geom})$-$(R_{grain\ boundary}Q_{grain\ boundary})$-$Q_{diffusion}$ at low temperatures or R_{bulk}-$(R_{grain\ boundary}Q_{grain\ boundary})$-$Q_{diffusion}$ at higher temperatures, where the bulk semicircle is no longer within the frequency window of the measurement.

7. Scanning electron microscopic characterization

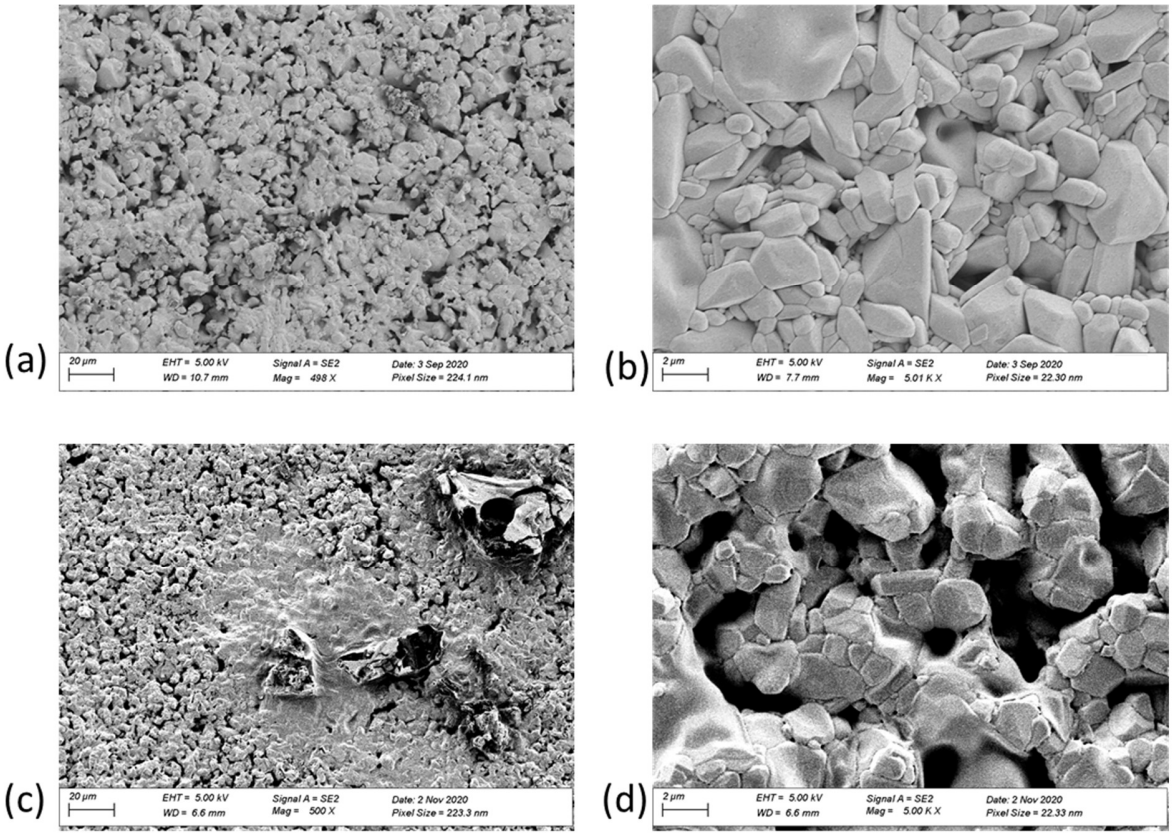

Figure S8. Scanning Electron Microscopy images of LTPO sintered for 10h (a) at magnification of 200 and (b) at magnification of 5000. SEM image of LTPO sintered for 14h (b) at magnification of 200 and (b) at magnification of 5000.

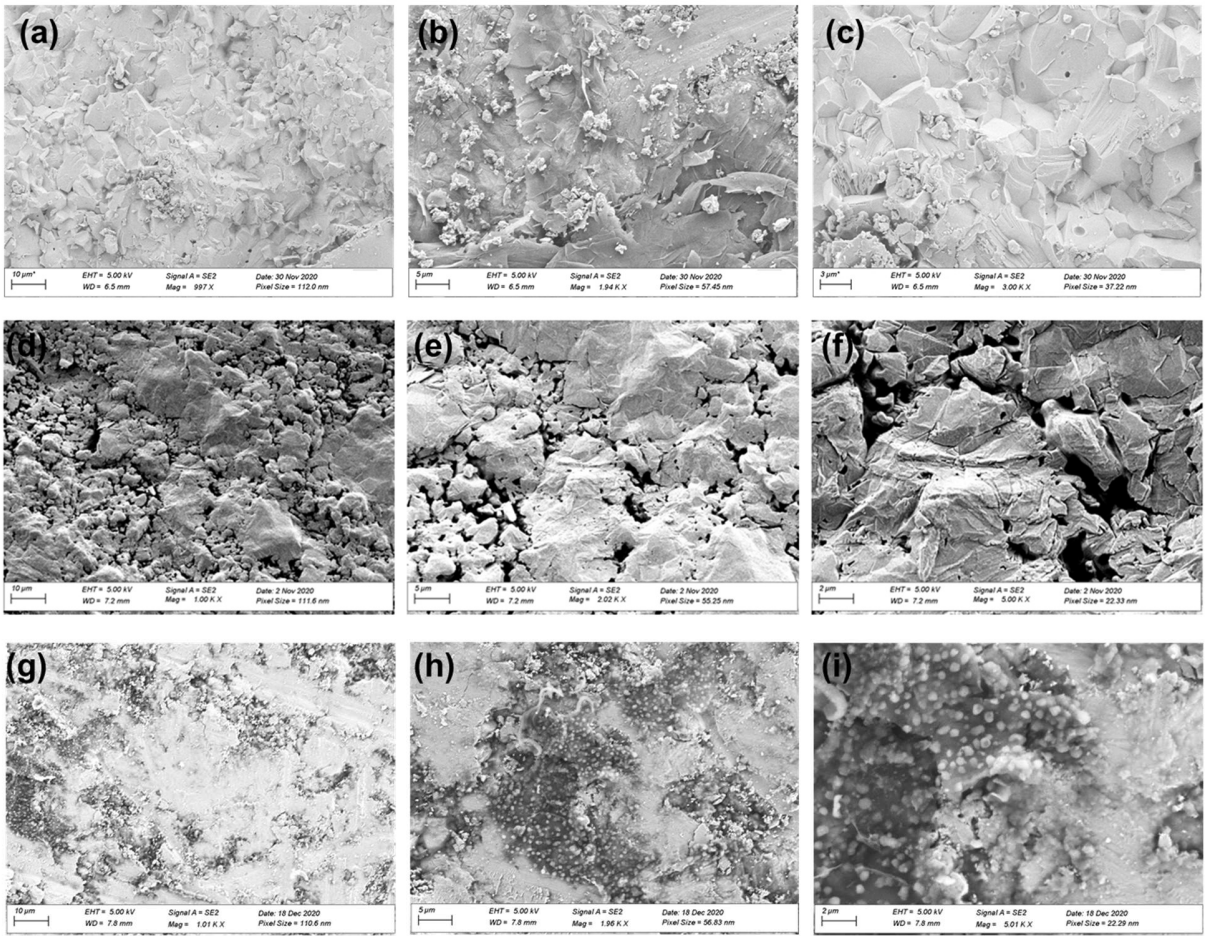

Figure S9. Scanning Electron Microscopy images of LTPO prepared by SPS at 1273 K, 30Mpa for 8 mins (a-f) or 4 min (g-i) under magnifications of (a,d,g) 1000, (b,e,h) 2000, (c) 3000 and (d,e) 5000. Dense samples in row 1 and 3 were from the same batch as those characterized by impedance. The SEM micrographs (d,e,f) of a damaged region of another 1273K_30MPa_8min sample demonstrate the hazard of uneven grain growth on excessive spark plasma sintering. Small crystallites on the surface of the 1273 K_30Mpa_4 min sample show some Li_2CO_3 re-formed on cooling the sample in humid air.

8. Cell voltage variation of Li|LE|LTPO|LFP cell

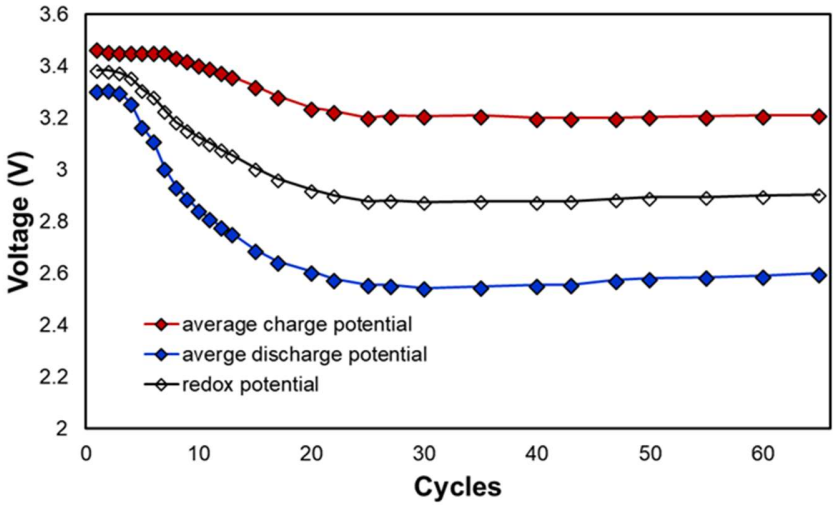

Figure S10. Evolution of average cell voltage during charging (red diamonds) and discharging (blue diamonds) as well as average redox potential (open symbols) of the hybrid Li|LE|LTPO|LFP cell shown in Figure 11 over its cycle life at C/20.